Supplementary Information

Equations

The following equation 1 and equation 2 are used for the ratio of diffusion-controlled and capacitive contribution:

$$i = av^b \quad (1)$$

$$i(V) = k_1 v + k_2 v^{1/2} \quad (2)$$

By rewriting the above equations and simplifying them, we get the follow equations:

$$\log(i) = b\log(v) + \log(a) \quad (3)$$

$$i(V)/v^{1/2} = k_1 v^{1/2} + k_2 \quad (4)$$

The equation (3), in which i represents the peak current, v represents the scan rate, and a and b represent the adjustable parameters, can be used to determine the Li^+-diffusion lithiation type instead of pseudocapacitive behavior. In equation(4), v, i, $k_1 v$, and $k_2 v^{1/2}$ represent scan rate, current, and contributions of capacitive and diffusion-controlled behavior, respectively. The values of k_1 and k_2 can be quantified as the contributions of capacitive and diffusion-controlled behaviors.

The diffusion coefficient computational formula is as follows:

$$D^{GITT} = \frac{4}{\pi\tau}\left(\frac{m_B V_M}{M_B S}\right)^2\left(\frac{\Delta E_s}{\Delta E_t}\right)^2$$

where τ is the time for a corresponding galvanostatic current; m_B, M_B, and V_M are the mass, molecular weight, and molar volume of THP, respectively; S is the electrode–electrolyte interface area (taken as the geometric area of the electrode); ΔE_s and ΔE_t are the voltage difference in one relaxation time and the voltage difference during one current pulse, respectively.

Supporting Figures and Tables

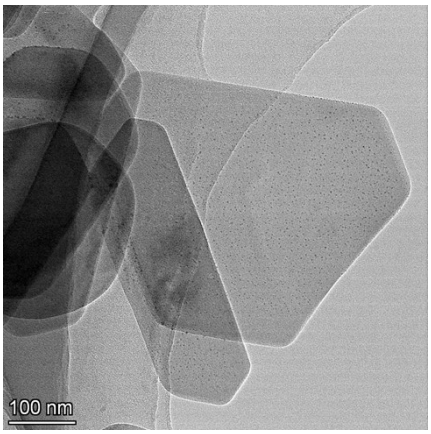

Fig. S1 TEM images of the THP.

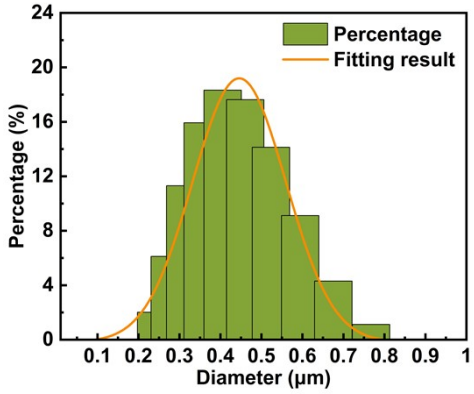

Fig. S2 The granularity distribution and average diameter of particles of synthesized THP.

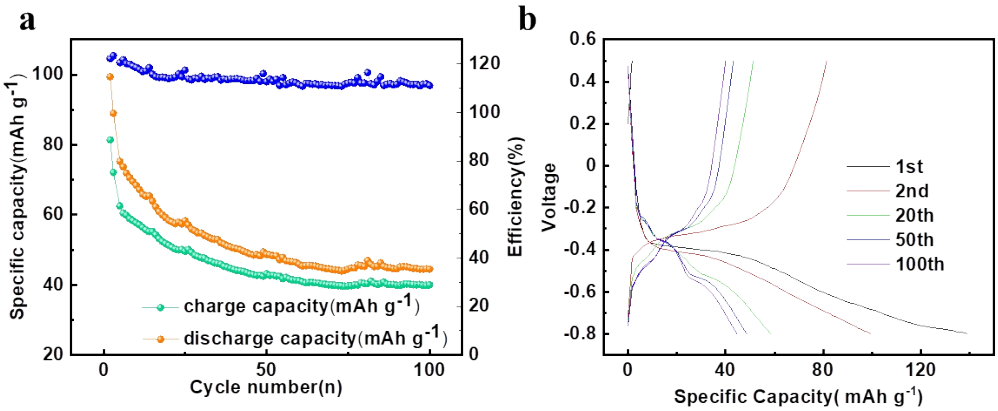

Fig. S3 (a) The cycle performance of THP electrode at a current density of 0.1 A g^{-1}

and (b) the 1st, 2nd, 20th, 50th and 100th charge/discharge curves in a voltage range of -0.8 to 0.5 V vs. Ag/AgCl.

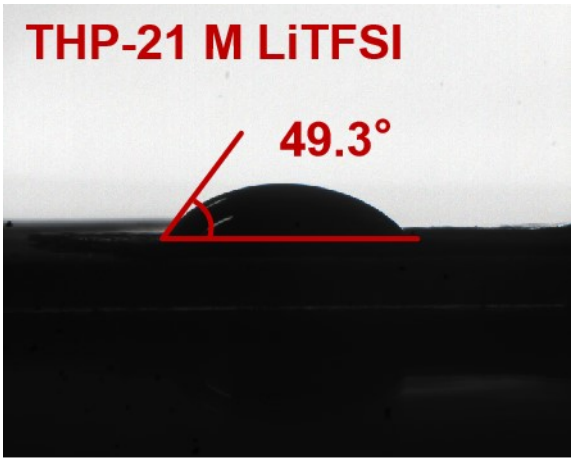

Fig. S4 Contact angle measurement of THP electrode with 21 m LiTFSI electrolyte.

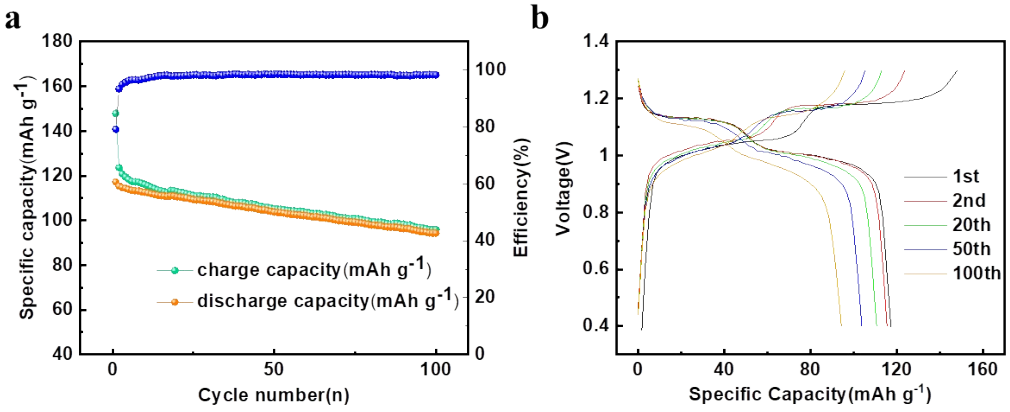

Fig. S5 (a) The cycle performance of LMO electrode at a current density of 0.1 A g^{-1} and (b) the 1st, 2nd, 20th, 50th and 100th charge/discharge curves in a voltage range of 0.4 to 1.3 V vs. Ag/AgCl.

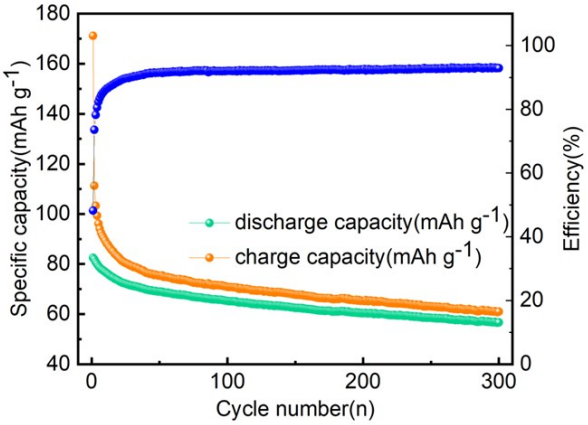

Fig. S6 Long-term cycle performance of LMO//1 m LiTFSI//THP full cell electrode at 0.05 A g^{-1}.

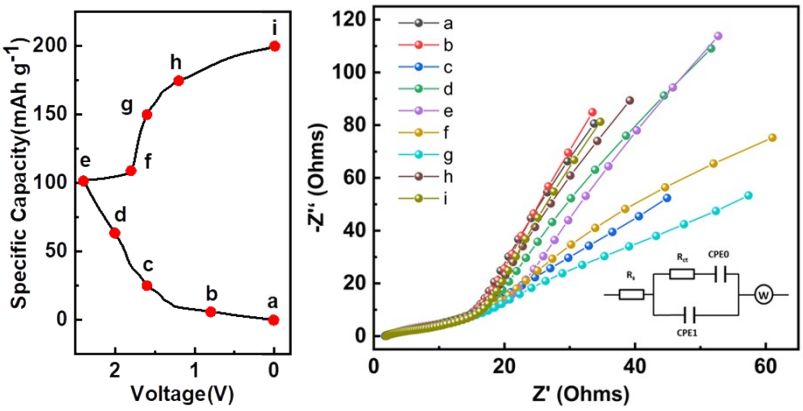

Fig. S7 ex situ impedance spectra of THP//LMO at different voltage during charging and discharging process between 100 kHz and 0.01 Hz in different cycles at 0.05 Ag-1. The states measured by ex situ impedance spectra (right) are represented by the marked dots (a to i) in the GCD curves (left).

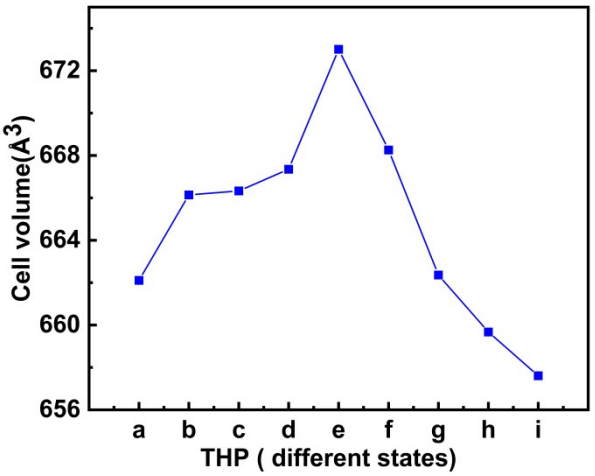

Fig. S8 The corresponding cell volume change of the anode during charging and discharging at different states (Li^+ insertion/extraction).

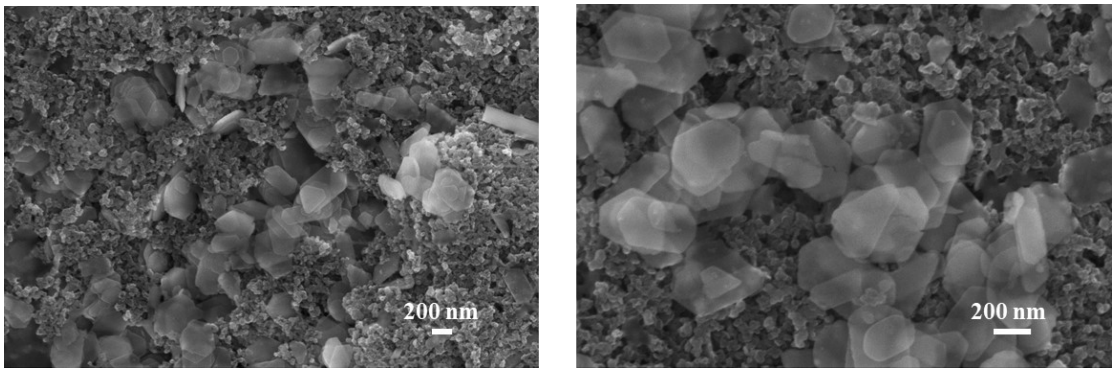

Fig. S9 SEM images of THP anode after 100 cycles.

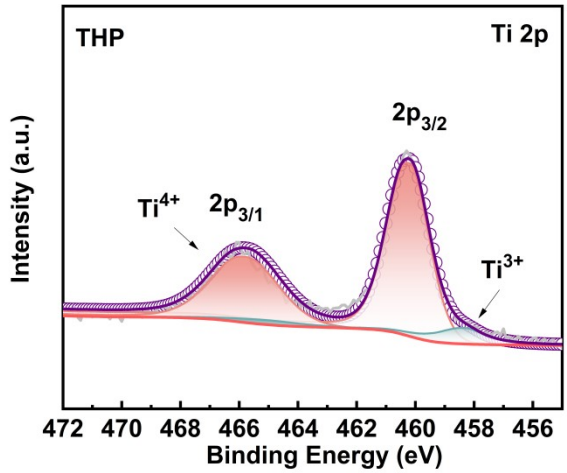

Fig. S10 Ti 2p XPS spectra of pristine THP sample.

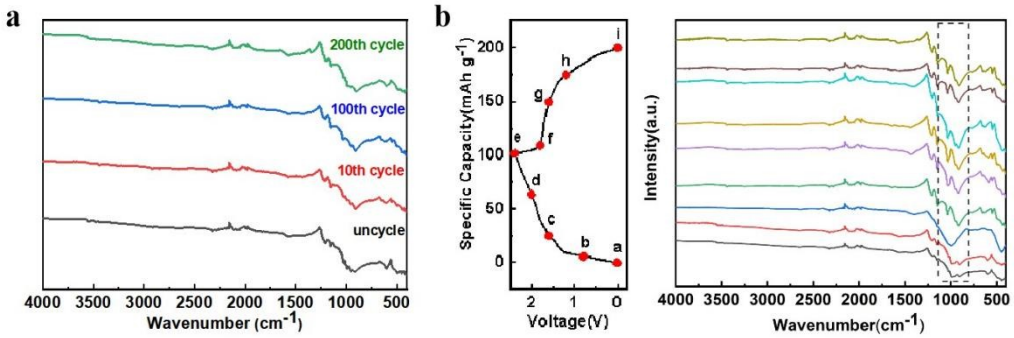

Fig.11 (a) FT-IR spectra of THP electrode after different cycles. (b) The ex situ FT-IR patterns of THP in the full ARLB at different states; the cells were first cycled for 15 cycles then charged/discharged to the desired states at 0.05 A g^{-1}.

Table S1 the simulation results of Rct and Zw

Sample	a	b	c	d	e	f	g	h	i
Rct (Ω)	7.96	7.73	7.40	8.29	11.8	21.4	6.95	7.73	8.89
ZW(DW)	19.2	19.9	29.7	33.0	34.9	21.5	42.0	26.1	19.4

Table S2 various rechargeable aqueous lithium battery

Cell Type	Electrolyte	electrochemical window	Initial Capacity (mAh g^{-1})	Capacity retention (%)	Ref.
$LiMn_2O_4$||LiV_3O_8 nanowires	saturated $LiNO_3$	0.5-1.5 V	103.9 mAh g^{-1}	83 %(100)at 0.15 A g^{-1}	[1]
$LiMn_2O_4$||TiS_2	21 M LiTFSI	0.7-2.2V	58 mAh g^{-1}	74 %(50) at 1 C	[2]
$LiMn_2O_4$||VO_2 (D)	2 M Li_2SO_4	0.2-1.8 V	97.4 mAh g^{-1}	35 %(1000)at 0.1 A g^{-1}	[3]
$LiMn_2O_4$||$(NH_4)_2V_7O_{16}$	2 M Li_2SO_4	0.01-1.7 V	38.6 mAh g^{-1}	78 %(500) at 0.3 A g^{-1}	[4]
$LiMn_2O_4$||$LiTi_2(PO_4)_3$@carbon	2 M Li_2SO_4	0-1.85 V	97 mAh g^{-1}	72 %(200) at 0.2 C	[5]
$LiMn_2O_4$||$LiTi_2(PO_4)_3$@graphene			107.6 mAh g^{-1}	88 %(200) at 0.2 C	
$LiMn_2O_4$||$FePO_4 \cdot 2H_2O$	15 M LiTFSI	0-1.9 V	82 mAh g^{-1}	92 %(500) at 0.2 C	[6]
$LiMn_2O_4$||$FePO_4$			163 mAh g^{-1}	71 %(300) at 0.2 C	
$LiMn_2O_4$||$LiTi_{2-x}Sn_x(PO_4)_3$/C	saturated $LiNO_3$	0-1.85 V	118 mAh g^{-1}	77%(1000) at 10 C	[7]
$LiMn_2O_4$||PANI	saturated $LiNO_3$	0.5-1.5 V	110.4 mAh g^{-1}	81%(150) at 0.075 A g^{-1}	[8]
$LiMn_2O_4$||C–TiP_2O_{7-y}	1 M Li_2SO_4	0.5-1.7 V	97 mAh g^{-1}	85%(800) at 0.1 A g^{-1}	[9]
$LiMn_2O_4$||TiP_2O_7/C	2 M Li_2SO_4	0-1.85 V	98 mAh g^{-1}	91%(100) at 0.25 C	[10]
$Li[Co_{1/3}Ni_{1/3}Mn_{1/3}]O_2$||$Li_2FeSiO_4$/C	1 M Li_2SO_4 + 1 M LiOH	0.5-1.55 V	89.8 mAh g^{-1}	>90%(30) at 0.01 A g^{-1}	[11]
$LiMn_2O_4$||$Ti(HPO_4)_2 \cdot H_2O$	21 M LiTFSI	0-2.4 V	119 mAh g^{-1}	83%（500）at 0.1 A g^{-1}	This work

Reference

1. J. Liu, L. Yi, L. Liu and P. Peng, *Mater. Chem. Phys.*, 2015, **161**, 211-218.
2. W.-X. Song, H.-S. Hou and X.-B. Ji, *Acta Physico-Chimica Sinica*, 2017, **33**, 103-129.
3. Y. Ma, D. Zhu, H. Zhou, Y. Tang, C. Hu, X. Meng, X. Jin, T. Xu and X. Cao, *J. Alloys Compd.*, 2023, **930**.
4. Y. Ma, M. Wu, X. Jin, R. Shu, C. Hu, T. Xu, J. Li, X. Meng and X. Cao, *Chem. Eur. J.*, 2021, **27**, 12341-12351.
5. Z. Zhou, W. Luo, H. Huang, S. Huang, Y. Xia, N. Zhou and Z. He, *Ceram. Int.*, 2017, **43**, 99-105.
6. Y. Wang, S.-Z. Yang, Y. You, Z. Feng, W. Zhu, V. Gariepy, J. Xia, B. Commarieu, A. Darwiche, A. Guerfi and K. Zaghib, *ACS Appl. Mater. Interfaces*, 2018, **10**, 7061-7068.
7. Z. He, Y. Jiang, J. Zhu, Y. Li, Z. Jiang, H. Zhou, W. Meng, L. Wang and L. Dai, *J. Alloys Compd.*, 2018, **731**, 32-38.
8. L. Liu, F. Tian, M. Zhou, H. Guo and X. Wang, *Electrochim. Acta*, 2012, **70**, 360-364.
9. D. Bin, Y. Wen, Y. Yuan, Y. Liu, Y. Wang, C. Wang and Y. Xia, *Electrochim. Acta*, 2019, **320**, 134555.
10. P. Liu, Y. Ren, X. Huang, Y. Dai, X. Liu, D. Sun, H. He, Y. Tang and H. Wang, *Electrochim. Acta*, 2018, **278**, 42-50.
11. W. Chen, M. Lan, D. Zhu, C. Ji, X. Feng, C. Yang, J. Zhang and L. Mi, *J. Mater. Chem. A*, 2013, **1**, 10912-10917.